

## Investigation of the high-strain rate (shock and ballistic) response of the elastomeric tissue simulant Perma-Gel®

G. J. Appleby-Thomas<sup>1,\*</sup>, D. C. Wood<sup>1</sup>, A. Hameed<sup>1</sup>, J. Painter<sup>1</sup>, V. Le-Seelleur<sup>1</sup> and B. C. Fitzmaurice<sup>1</sup>

<sup>1</sup>Centre for Defence Engineering, Cranfield University, Defence Academy of the United Kingdom, Shrivenham, SN6 8LA

**Keywords:** Perma-Gel®; Tissue Simulant; Shock; Ballistic impact; Equation-of-state

### ABSTRACT

For both ethical and practical reasons accurate tissue simulant materials are essential for ballistic testing applications. A wide variety of different materials have been previously adopted for such roles, ranging from gelatin to ballistics soap. However, while often well characterised quasi-statically, there is typically a paucity of information on the high strain-rate response of such materials in the literature. Here, building on previous studies by the authors on other tissue analogues, equation-of-state data for the elastomeric epithelial / muscular simulant material Perma-Gel® is presented, along with results from a series of ballistic tests designed to illustrate its impact-related behaviour. Comparison of both hydrodynamic and ballistic behaviour to that of comparable epithelial tissues / analogues (Sylgard® and porcine muscle tissue) has provided an insight into the applicability of both Perma-Gel® and, more generally, monolithic simulants for ballistic testing purposes. Of particular note was an apparent link between the high strain-rate compressibility (evidenced in the Hugoniot relationship in the  $U_s$ - $u_p$  plane) and subsequent ballistic response of these

\*Corresponding author. Tel. +44 (0) 1793 78571. Email address:  
[g.applebythomas@cranfield.ac.uk](mailto:g.applebythomas@cranfield.ac.uk)

materials. Overall, work conducted in this study highlighted the importance of fully characterising tissue analogues – with particular emphasis on the requirement to understand the behaviour of such analogues under impact as part of a system as well as individually.

## **1. Introduction**

Living systems are extremely complex in construction – e.g. the multi-layered nature of mammalian tissue comprising bone, muscle tissue, etc. Consequently, prediction of the effects of ballistic insults on living targets is extremely challenging. Factors ranging from the nature of the attack, any protection present to the aforementioned complexity of the target can all contribute to the resultant effects. Ballistic trials offer one route to understand such phenomena. These are, however, both time and resource intensive leading to high capital costs, not least as different trials would be required for differing projectile / armour / tissue configurations. Instead, numerical simulation via the use of explicit dynamic hydrocodes provides a more economic route to interrogate such behaviour. However, the validity of such an approach necessitates understanding of material hydrodynamic and constitutive equations-of-state for all elements involved. While a substantial body of research exists on the high-rate properties of munition [1] and armour-relevant [2, 3] materials, there is less information available on the dynamic response and associated damage mechanisms in both tissues and potential analogues.

Such equation-of-state data requires experimental derivation. In addition, for ballistic testing purposes, a combination of availability and ethical considerations mean that such experiments will likely involve analogues instead of real-world mammalian tissue samples. Common

examples of such simulants include (the monolithic materials) ballistics gelatin [4-6] and soap [7-9]. However, as touched on above, real-world tissue structures typically comprise multiple (often anisotropic) layers. These range from the epidermis and dermis (skin) through subcutaneous fat (adipose tissue) and muscle layers down to the underlying bone/structural elements [10-13]. Consequently, the use of bulk and (typically) homogenous tissue simulants such as gelatin or soap is necessarily an approximation. The importance of understanding multiple simulant materials is further emphasised by the fact that tissues are known to exhibit a high degree of strain-rate sensitivity [12], making it unlikely that any single simulant material would suffice to simulate dynamic behaviour under impact. In general, there are a number of core areas which a simulant could potentially mimic, namely: epithelial (lining), muscular, connective (interfacial) and skeletal (supporting) tissues [14]. To this end, building on previous work in this area, here the high strain-rate response of an emerging bulk [15, 16] and brain [17] tissue analogue – Perma-Gel® – is considered. There is a relative paucity of data on this material available in the literature, with – to the author’s knowledge – only limited ballistic and low strain-rate studies and no high strain-rate data.

With regards to ballistic testing, there have been a very-limited number of studies on this material to-date [15, 16]. In the first of these studies, Ryckman et al. [15] carried out a series of ballistics tests accelerating 0.5-inch-diameter chrome steel spheres at 200 to 900 feet-per-second (60 to 275 m/s) into Perma-Gel® targets using a compressed gas-gun. Observation of the impact event using a high-speed camera as well as of post-impact recovered targets provided a number of insights into Perma-Gel’s® behaviour. Of particular note was the elastomeric response of Perma-Gel®; temporary cavities were observed to form along the penetration path and then collapse back about instabilities / perturbations. Initial penetration was also observed to exhibit a relatively constant initial velocity before a subsequent pull-

back to a final depth of penetration significantly less than the peak depth. Such behaviour is consistent with the elastomeric behaviour observed previously in the polymeric material polycarbonate replacement resin [18], where the pull-back from peak penetration depth was associated with the release of stored elastic strain-energy ahead of the impacting projectile. The apparent nominally hydrodynamic (constant penetration velocity) is also of note – suggesting that accurate prediction of penetration will require hydrocodes and associated equation-of-state information. Interestingly, penetration was also found to trend above that which might be expected of 10 wt.% ballistics gelatin for impact velocities greater than c.a. 500 m/s. In similar work, in the only other study of note on the ballistic behaviour of Perma-Gel® apparent in the literature, Mabbott et al. [16] carried out a series of tests in which the ballistic response of Perma-Gel® was compared directly to that of 10 and 20 wt.% gelatin. In this study, 5.5-mm diameter ball bearings were accelerated to impact velocities of between 150 and 1,050 m/s (representative of handgun through-to high velocity rifle ammunition impact velocities). Rather than use a gas-gun to accelerate the projectile, however, Mabbott et al. employed a proof barrel on a small arms range, encasing the ball bearing projectiles in a polymeric sabot, itself emplaced within a 6.62 mm 51 mm cartridge case before firing. Comparison of resultant projectile depths-of-penetration in Perma-Gel® to that in the gelatin targets showed reasonable agreement between the Perma-Gel® and 10 wt.% material, albeit with an undershoot compared to the gelatin in the measured penetration at impact velocities below c.a. 400 m/s and an overshoot above (in line with the study by Ryckman et al. [15]).

While to-date there have been no high strain-rate studies of the behaviour of Perma-Gel®, there have been some limited low strain-rate investigations into its dynamic properties. For example, in a recent paper Kalcioglu et al. [19] used a nano-indenter to investigate the indentation response of Perma-Gel® as well as a series of styrenic block co-polymers,

comparing resultant material mechanical response to that of real (rat heart and lung) tissues. While tests were carried out at relatively low strain-rates (impact velocities of the order of 10's of mm/s), it was noted that the use of small indenters allowed strain energy densities comparable to ballistic events to be achieved. Analysis of indentation depths showed that Perma-Gel® broadly mimicked real tissue response at low strain energy densities, but became less comparable as the loading mass increased. A marked strain-rate sensitivity was apparent in all materials considered – with Perma-Gel® exhibiting a response intermediate to the co-polymers tested (likely due to having a similar composition to these materials [17]). In addition, the rate of energy dissipation was considered, with Perma-Gel® again found to produce a result dissimilar to the real materials. Overall, while strain-rates considered were not comparable to those likely to be encountered during ballistic events, the discrepancy between actual tissue and analogue material dynamic response highlights the importance of a deeper understanding of simulant behaviour beyond just ballistic testing. In similar work, but over a larger range of strain-rates (up to 100/s), Pervin and Chen [17] investigated the dynamic behaviour of both Perma-Gel®, collagen gel and a series of different Agrose gels (with the research concentrated on the latter). Dynamic Mechanical Analysis (conducted at 30°C over 0.1-100 Hz with a 15 µm amplitude and 1% strain) and hydraulically-driven compression tests were carried out on the different materials, with results compared to those of Bovine white brain matter. As with Kalcioglu et al. [19] a noticeable strain-rate dependency in the mechanical response of Perma-Gel® was found. In addition, as with the study comparing behaviour to heart and lung tissue, here the dynamic response of Perma-Gel® was again not the best fit to the brain-tissue of the analogues considered.

While the studies above consistently showed that Perma-Gel® was not an exact analogue to the tissues considered, it is worth noting that the form – if not the exact magnitudes achieved – of the measured energy absorption rate [19], stress-strain response [17], etc were typically comparable to that of the real tissues. Consequently, it is arguable that as long as Perma-Gel® is well characterised it could be employed in a simulant role (e.g. with account taken of the different elastic-plastic response under load).

However, the limited studies outlined above have focused largely on the low strain-rate and / or ballistic response of Perma-Gel®; there is an even more marked paucity of data when it comes to higher rates of strain. Consequently, here, an investigation into the underlying high strain-rate material properties of Perma-Gel®, backed by simplified ballistic tests, has been undertaken in order to build on this previous work. In particular, the aim of these studies is to extend the knowledge of the high strain-rate response of Perma-Gel® into regions comparable to those likely to be observed about the tip of an impacting bullet.

The plate-impact technique [6, 20, 21] allows a one-dimensional state of strain to be established in target materials. This is achieved by launching a flat and parallel flyer plate at a measured velocity into a target whose surfaces perpendicular to the impact axis are also machined flat and parallel. The resultant high-rate loading generates a compressive shock within the target due to inertial confinement of material in the target centre. This leads to a one-dimensional loading which is maintained until arrival of rarefactions (release waves) from external edges [20]. It should be emphasised that a state of one-dimensional strain ( $\epsilon$ ) but not stress ( $\sigma$ ) is established, as detailed in:

$$\varepsilon_x \neq \varepsilon_y = \varepsilon_z = 0 \quad \text{and} \quad \sigma_x \neq \sigma_y = \sigma_z \neq 0 \quad (1)$$

Where the subscripts ‘x’ and ‘y’/ ‘z’ denote stress or strain as-appropriate along and orthogonal to the impact axis respectively (with the ‘y’ and ‘z’ directions are equivalent due to axial symmetry).

The propagation of such shocks is typically monitored via sensors such as embedded stress gauges [6, 21] or interferometers [22]. These sensors allow measurement of one or more of the five shock parameters, namely: the velocity of the propagating shock,  $U_S$ ; the mass/particle velocity of the continuum elements propagating the shock,  $u_p$ ; the Hugoniot – or longitudinal equilibrium – stress,  $\sigma_x$ ; density of the target material,  $\rho$ , and; internal target material energy,  $E$ . Additional shock parameters can then be calculated via the Rankine-Hugoniot conservation (jump) equations [20], with the accessible physical states a shocked material passes through described by Hugoniot relationships such as  $\sigma_x$ - $u_p$ . Here, the plate-impact technique has been employed to investigate the shock response of Perma-Gel® to allow derivation of a Hugoniot equation-of-state suitable for inclusion in hydrocode simulations. Further, this work – supported by limited ballistic tests – was designed to provide additional insight into the dynamic response of Perma-Gel®.

## 2. Material Properties

Perma-Gel® is a commercially available synthetic tissue simulant used for ballistic testing purposes. As a thermoplastic material it has the advantage of being able to be recast after testing and, in addition, does not suffer from biological degradation in the same way as more traditional simulant materials such as gelatin [15-17]. Compositional information is largely proprietary, but safety information from the supplier notes that key components are white mineral oil, gellants and a small (<1%) proportion of Butylated Hydroxy Toluene. Perma-Gel® is defined more precisely as a styrene-ethylene-butylene co-polymer by Pervin and Chen [17] – and was shown by Kalcioğlu et al. [19] to have broadly similar low strain-rate properties to selected other co-polymers of a similar composition to that suggested in Ref. [17].

Elastic longitudinal and shear wave speeds were measured using a Panametrics 5077PR pulse receiver in the pulse-echo configuration, with density measured by accurately weighing a cast specimen of known (cylindrical) geometry. Resultant values along with key calculated elastic properties are presented in Table 1. In addition, for the purpose of comparison, similar data from the literature is included for the simulant / tissue materials Sylgard® [23] and porcine muscle tissue [24]. In the latter case, data is the mean of (very similar) values presented in Ref. [24] for commercially-sourced and middle-white muscle tissue, with errors corresponding to the standard deviation in this calculated mean value.



**Table 1.** Key elastic material properties.

Material	Sound speeds (mm/ $\mu$ s)			$\rho_0$ (g/cc)	K (GPa)	$\nu$
	$c_l$	$c_s$	$c_0$			
Perma-Gel®	$1.42 \pm 0.01$	$0.38 \pm 0.01$	1.35 (calc.)	$0.87 \pm 0.05$	1.59 (calc.)	0.46 (calc.)
Sylgard®	$1.10 \pm 0.02$	$0.57 \pm 0.02$	0.88 (calc.)	$1.01 \pm 0.01$	0.78 (calc.)	0.32 (calc.)
Muscle tissue	$1.99 \pm 0.09$	$0.94 \pm 0.06$	$1.67 \pm 0.15$	$1.09 \pm 0.01$	3.04 (calc.)	0.36 (calc.)

### 3. Experimental Techniques

New experimental data for the epithelial tissue simulant Perma-Gel® are presented in this study. This data has been gathered via a combination of plate-impact (Hugoniot equation-of-state) and ballistic testing. In both cases single-stage compressed gas-guns were used to accelerate projectiles into targets in controlled laboratory conditions. In all cases Perma-Gel® was cast as-required into target elements following the manufacturers' instructions.

#### 3.1 Plate-impact tests

Plate-impact tests [1, 6, 20, 21] were employed to shock load the target material. Aluminium and copper flyer plates were launched at velocities in the range 340-933 m/s into Perma-Gel® targets using a 50-mm bore single-stage gas-gun. All projectile, target assembly and mounting faces perpendicular to the impact axis were finished to a tolerance of  $\leq 5 \mu\text{m}$ . This ensured (essentially) simultaneous contact between all elements of the flyer plate's surface and that of the target on impact, allowing inertial confinement within the target to be established.

The experimental arrangement for plate-impact targets is illustrated schematically in Fig. 1. Figure 1(a) shows an exploded form of the target package (comprising cover plate of identical material to the impacting flyer and associated encapsulated gauge, cast Perma-Gel® and rear gauge plus backing PMMA block), while Fig. 1(b) shows the muzzle end of gun with the target arrangement in-place.

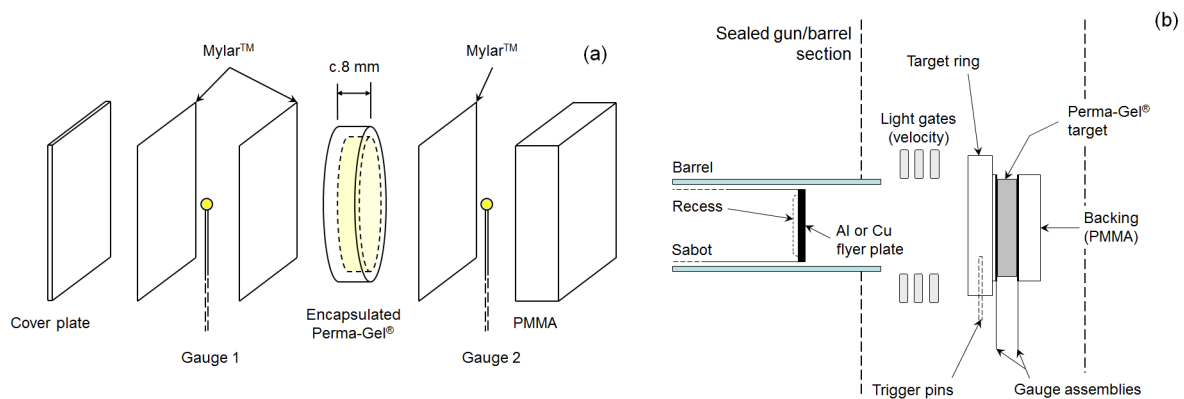


**Fig. 1.** Schematic illustration of plate-impact experimental setup elements: (a) exploded target configuration; (b) mounted target arrangement.

Flyer impact velocity was measured via a series of sequential light gates just prior to impact, with a pair of shorting trigger pins used to activate the gauge pulsed power supply plus recording oscilloscopes. The gauges (Fig. 1 – encapsulated by insulating 25  $\mu\text{m}$ -thick Mylar™) comprised longitudinal embedded manganin stress gauges (Vishay Micro-Measurements, USA) of type LM-SS-125CH-048. Gauge interpretation, based on the impedance matching technique [20], followed the approach adopted by Roserberg et al. [25].

### 3.2. Ballistic testing

In addition to plate-impact testing, a limited series of simplified ballistics tests were undertaken in order to interrogate the response of Perma-Gel® to impact. To this end, a series of four sphere impact (e.g. simplified projectile geometry) tests were carried out using a 22-mm bore single-stage gas-gun. Acetal sabot 12-mm diameter, 7.15 g, stainless steel projectiles were launched into 6-mm thick 190-mm diameter Synbone® (a polyurethane-based synthetic bone material) hemispherical targets. These targets, either empty or filled with Perma-Gel® or the alternate muscular tissue simulant Sylgard®, were adhered using a slow cure two-part epoxy (Loctite 3421 Hysol®) to 8-mm thick polycarbonate backing plates which were subsequently clamped vertically in the gun's target chamber. It should be noted that Sylgard® was primarily employed here as it has been previously extensively characterised by a selection of the authors of this paper [23]. While the filling simulant were of primary interest, in addition to the requirement to have a medium to cast the filling materials in to, it was considered appropriate to try and nominally simulate a 'skull-like' structure for these tests by employing a Synbone® outer casing. This approach also had the additional advantage of providing baseline data for future further studies of simulant materials (e.g. building on Refs. [6, 23]), while also – providing a ready comparison between the differing simulant materials considered here. The experimental arrangement is shown in Fig. 2. Just prior to impact sabots were stripped using a steel stripping arrangement, with the projectile subsequently travelling independently for c.a. 200 mm before impacting the target. Experiments were observed using a Phantom V12 high speed camera, with this footage also employed to determine the impact velocity of the projectile. In addition, careful analysis of recovered footage demonstrated that the target remained relatively stationary during the core part of the penetration process.

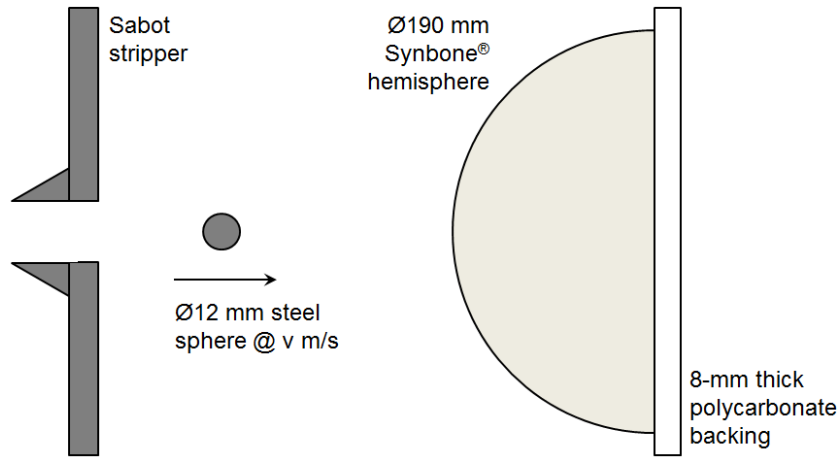


**Fig. 2.** Schematic illustration of ballistic testing experimental arrangement.

## 4. Results and Discussion

### 4.1. Plate-impact tests

A total of seven plate-impact experiments were conducted. Key shot parameters and resultant data are set out in Table 2.

**Table 2.** Summary of plate-impact experimental results.

Impact velocity (m/s)	Flyer plate			
	(thickness / material)	$u_p$ (mm/ $\mu$ s)	$U_s$ (mm/ $\mu$ s)	$\sigma_x$ (GPa)
340	10-mm Al	0.29	2.33	0.58
485	10-mm Al	0.41	2.69	1.13
619	10-mm Al	0.52	2.88	1.41
665	10-mm Cu	0.62	3.07	2.03 <sup>1</sup>
781	10-mm Cu	0.72	3.29	2.56
882	5-mm Cu	0.76	3.38	2.70 <sup>1</sup>
933	5-mm Cu	0.86	3.29	3.05 <sup>1</sup>

<sup>1</sup>Stress calculated from rear gauge via Eq. (2)

A typical pair of front and rear gauge traces are presented in Fig. 3. Wave / shock velocities were calculated based on the interval between shock arrival at the two gauges ( $\Delta t$  in Fig. 3) and knowledge of the gauge's spatial separation. In this figure, the rear gauge trace has been re-calibrated from stress in the backing PMMA to stress in the Perma-Gel® using the relation shown in:

$$\sigma_{Perma-Gel} = \frac{1}{2} \frac{(Z_{Perma-Gel} + Z_{PMMA})}{Z_{PMMA}} \sigma_{PMMA} \quad (2)$$

Where  $Z_x$  is the impedance of material 'x' (equal to density ( $\rho_0$ ) multiplied by wave velocity ( $U_s$ ) measured as shown in Fig. 3),  $\sigma_{Perma-Gel}$  is the stress in the Perma-Gel® and  $\sigma_{PMMA}$  the stress in the PMMA.

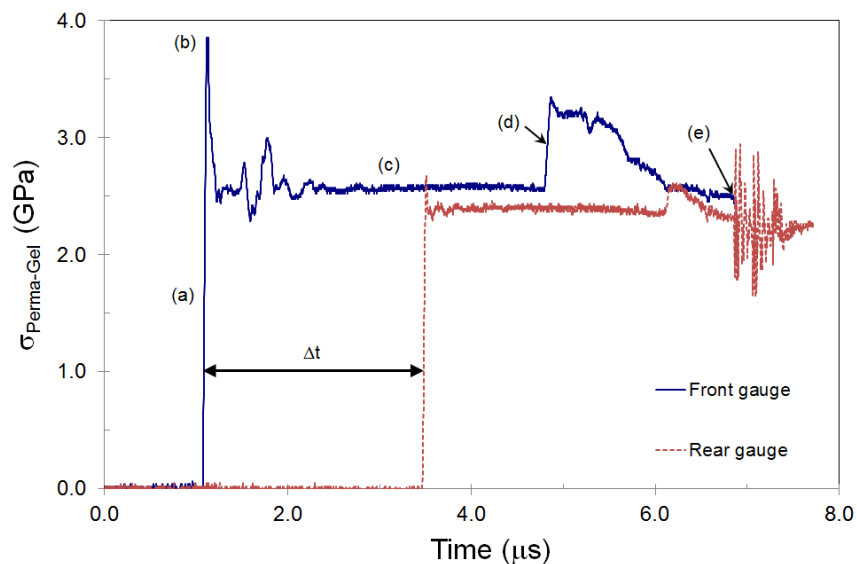


**Fig. 3.** Typical front and rear stress longitudinal gauge traces (781 m/s 10-mm Cu flyer shot from Table 2).

There are a number of features which are immediately apparent on observation of these traces. Following shock arrival a rapid (36.8 ns) rise occurs (a) leading to an overshoot in stress (b) which rapidly decays back – albeit in a noisy fashion – to a plateau (the Hugoniot stress) at (c). Such overshoots in stress have been attributed elsewhere to both the fast-rising nature of the shock itself [26] or, more physically, to capacitance-based electrical effects – likely induced as a metallic flyer approaches an insulated gauge [1]. However, the subsequent ringing may also be partially attributable to either a charging effect within the Perma-Gel® itself, or alternatively reflections from pores/air-pockets which may have resulted during material/target casting. Following the relatively constant Hugoniot plateau, a re-loading occurs at (d) due to shock reflection from the backing PMMA; subsequently stress decays as releases from the target outer edges catch up with the shock – with gauge death apparent by point (e). Similar features are apparent on the rear trace. In addition, interestingly, at the point at which the front gauge appears to die a significant burst of noise is apparent on the rear gauge – indicative of electrical cross-talk.

The resultant Hugoniot equation-of-state based on the data presented in Table 2 is shown in Fig. 4. Error bars have been introduced based on assessment of the maximum and minimum potential shock arrival times on recorded traces following an approach previously adopted elsewhere [1]. Essentially, the earliest possible shock front arrival at the front gauge combined with the latest possible arrival at the rear gauge leads to the lowest potential shock velocity and vice-versa. From this range of shock velocities, a corresponding range of particle-velocities were calculated via the impedance matching technique based on knowledge of the flyer material properties and impact speed [20]. In addition, for

comparison, equation-of-state data for both Sylgard® [23] and porcine muscle tissue [24] are also included in this figure (although, in the case of the porcine muscle data, following on from a discussion detailed below / in Table 3, a non-linear fit to experimental data from Ref. [24] is included here).

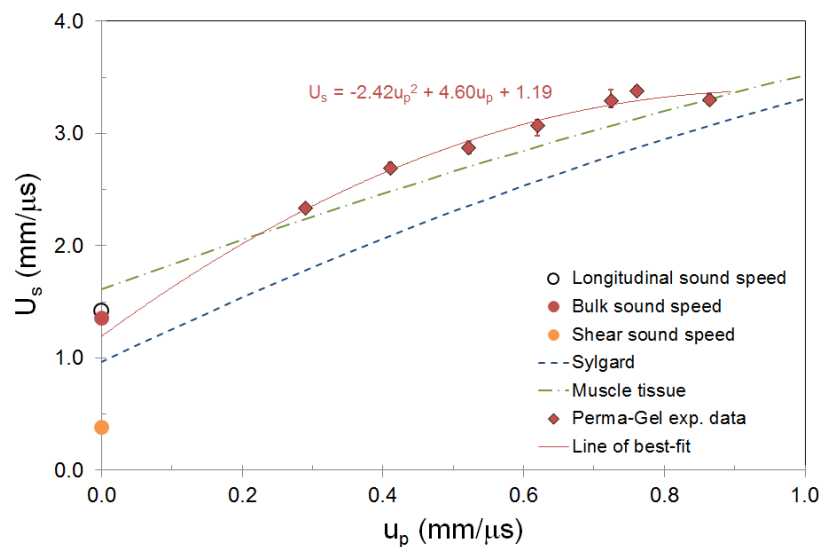


**Fig. 4.**  $U_s$ - $u_p$  equation-of-state for Perma-Gel® plus literature data for Sylgard® [23] and porcine muscle.

A clear non-linear response is apparent in the  $U_s$ - $u_p$  plane for Perma-Gel®. Such behaviour has been observed elsewhere for polymeric materials such as epoxy resins [27] and PMMA [28, 29] – as well as in Sylgard® [23] as shown Fig. 4. This type of non-linear response has been attributed to the complex structure of polymeric materials [29]. Essentially, compression is believed to occur preferentially along the weaker bonds lying perpendicular to the polymer chains, with the stiffer inter-chain bonds compressing more slowly. Consequently, such compression will be a multi-stage process, leading to the observed curvature in the  $U_s$ - $u_p$  plane.

While a non-linear fit appears appropriate for Perma-Gel® and Sylgard® in Fig. 4, the Hugoniot equation-of-state for muscle tissue is much closer to a linear form, to the extent that it is noted as having a linear nature of the form  $U_s = c_0 + Su_p$  in Ref. [24]. Here, however, as detailed in Table 3, on re-examination of the data a non-linear fit was found to be preferable – however, the difference is nominal. For linear  $U_s$ - $u_p$  equations-of-state, the intercept with the ordinate typically corresponds to the materials bulk sound speed, while the slope (S) has been linked to the compressibility of a given material; e.g. as the first pressure derivative of the bulk modulus, the higher the magnitude of ‘S’, the higher the materials compressibility [30-32]. To this end, both linear and non-linear best-fits (derived via the least-squares fitting function in Microsoft Excel™) along with associated residual ‘R<sup>2</sup>’ values are presented for the three materials considered here in Table 3. There are two features which are immediately of note from this data. Firstly, while as detailed above a non-linear fit to experimental data from Ref. [24] has been employed here, the linear fit in fact has a comparable R<sup>2</sup> value of 0.9653 instead of 0.9666 for the non-linear case. However, this is a relatively small difference suggesting – within experimental error – that a linear fit would suffice. The second feature which emerges from Table 3 is the variation in compressibility between the three simulant materials considered here. Perma-Gel® appears to have a broadly comparable compressibility to muscle tissue, suggesting it may be a reasonable analogue for such tissue (S equal to 1.81 and 1.89 respectively; for comparison, S for gelatin has been shown elsewhere to be c.a. 1.77 [23]). However, Sylgard®, which has found application – like Perma-Gel® – as an epithelial or muscular (brain) simulant material has a markedly greater apparent compressibility under high strain-rate loading (S equal to 2.45). This result suggests that Sylgard® possesses a heavily cross-linked nature. Complex (heavily cross-linked, or large side-grouped) polymeric structures have been shown elsewhere to ‘harden’ behind a shock as steric effects become dominant [32-34]; such a response would be lacking in the



simpler / more homogenous Perma-Gel® and muscle tissue which might arguably be expected to show a consistency closer to that of an incompressible fluid.

**Table 3.** Best-fit equations-of-state for Perma-Gel®, Sylgard® [23] and Muscle tissue [24] (data based on Fig. 4).

Material	Equations-of-state	R <sup>2</sup>
Perma-Gel®	$U_S = 1.91 + 1.81u_p$	0.9329
	$U_S = 1.20 + 4.60U_p - 2.42U_p^2$	0.9784
Sylgard®	$U_S = 1.03 + 2.45u_p$	0.9855
	$U_S = 0.96 + 3.03U_p - 0.68U_p^2$	0.9898
Muscle tissue	$U_S = 1.69 + 1.89u_p$	0.9653
	$U_S = 1.61 + 2.29U_p - 0.38U_p^2$	0.9666

In addition to the above discussion of the compressibility of the analogue materials considered here, it is also immediately apparent from Fig. 4 that Perma-Gel® is behaving differently under shock compression to the other two tissue simulant / materials considered – namely Sylgard® and porcine muscle tissue. However, at elevated particle-velocities there appears to be some evidence that the Perma-Gel® data is trending towards the muscle tissue response. Such potential convergence is also apparent in the  $\sigma_x$ - $u_p$  plane as shown in Fig. 5 (based on the data presented in Table 2). Here, as with the  $U_S$ - $u_p$  data in Fig. 4, Hugoniot equations-of-state for both Sylgard® and porcine muscle tissue are again included for comparison. These have been calculated via Eq. (3) [37] based on the  $U_S$ - $u_p$  curves presented in Fig. 4 and Table 3.

$$\sigma_x = \rho_0 U_s u_p \quad (3)$$

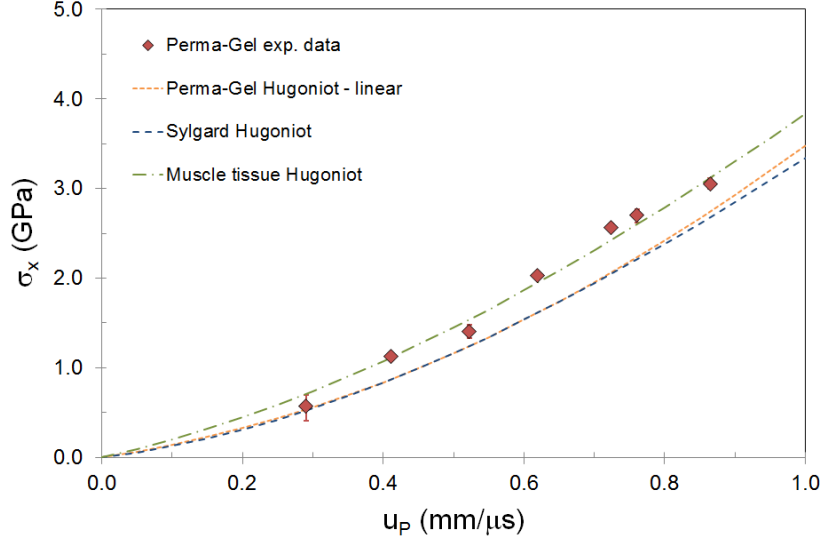


**Fig. 5.**  $\sigma_x$ - $u_p$  equation-of-state for Perm-Gel® plus literature data for Sylgard® [23] and porcine muscle tissue [24].

As with the  $U_s$ - $u_p$  data presented in Fig.4, in Fig. 5 the Perma-Gel® experimental data is again observed to be trending towards the corresponding muscle equation-of-state. In addition, it is interesting to note that the experimental data points for Perma-Gel® are observed to nominally trend above the corresponding hydrodynamic response (the Hugoniot) – which was calculated via Eq. (3) based on the (non-linear)  $U_s$ - $u_p$  curve presented in Fig. 4 / Table 3. While elsewhere such behaviour has been tentatively linked to steric-based strengthening effects behind the shock [33, 35, 36], here further observation suggests that the deviation is in fact relatively insignificant. In Fig. 6(a) and (b), data is presented in both the  $\sigma_x$ - $u_p$  and  $\sigma_x$ - $v$  planes respectively. In these cases a best-fit to the experimental data from Ref. [24] for porcine muscle tissue (where such experimental deviation from the hydrodynamic response had been judged minimal) is included alongside the experimental data presented here for Perma-Gel® as well as the corresponding Hugoniot curves for both the linear and non-linear cases calculated using Eq. (3) and presented in Table 3. Further, an

additional fit representing the resultant behaviour when the  $U_s$ - $u_p$  curve in Fig. 4 is taken through the bulk sound speed from Table 1 (taking the form  $U_s = 1.35 + 2.66u_p$ ,  $R^2 = 0.71$ ) is also included for comparison. For the data presented in the  $\sigma_x$ - $v$  plane in Fig. 6(b), volumes ( $v$ ) were calculated from the data presented in Table 2 according to Eq. (4), where  $v_1$  is the final volume / state obtained under shock and  $v_0$  is the initial volume [20].

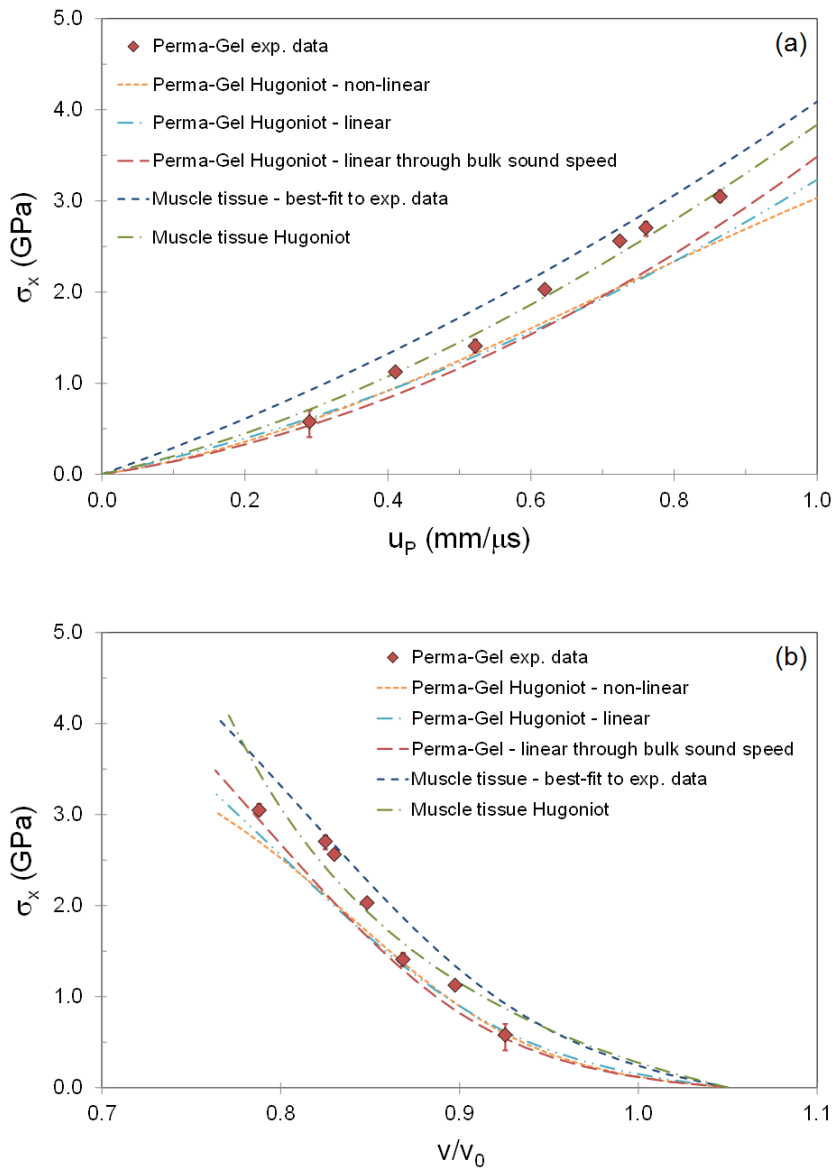


**Fig. 6.** Hugoniot equations-of-state plus experimentally measured stresses for Perma-Gel® and porcine muscle tissue [24] (a)  $\sigma_x$ - $u_p$  and (b)  $\sigma_x$ - $v$ .

$$\frac{v_1}{v_0} = \frac{U_s - u_p}{U_s} \quad (4)$$

From Fig. 6(a) it is apparent that to a reasonable first order, muscle tissue essentially exhibits a broadly hydrodynamic or fluid-like response with all experimental data broadly sitting on the Hugoniot curve (although, some deviation from the hydrodynamic response was found at certain stresses [24]). Overall, the deviation between the Perma-Gel® – as highlighted previously in Fig. 5 – is relatively comparable in extent to that of the porcine muscle tissue experimental data from its corresponding Hugoniot. Further, it is apparent that the highest particle velocity / pressure data point for the Perma-Gel® material in fact sits relatively close to the linear Hugoniot curve. This effect is even more marked when the data is considered in the  $\sigma_x$ - $v$  plane as shown in Fig. 6(b), where the highest particle velocity Perma-Gel® data point falls exactly on the corresponding linear Perma-Gel® Hugoniot, particularly for the fit corresponding to that through the bulk sound speed in Fig. 4. On this front, it is interesting to note the variation at higher up values in both Fig. 6(a) and (b) in terms of the influence of the  $U_s$ - $u_p$  fit from Fig. 4 employed to calculate the  $\sigma_x$ - $u_p$  and  $\sigma_x$ - $v$  curve via Eq. (3) respectively. Consequently, Fig. 6 therefore suggests that the discrepancy between the calculated Hugoniot and experimentally measured longitudinal stress values for Perma-Gel® is likely primarily a function of the influence of the non-linearity of the  $U_s$ - $u_p$  Hugoniot on the subsequently calculated the  $\sigma_x$ - $u_p$  Hugoniot curve. Further, it is worth noting the fact that the Perma-Gel® targets were cast individually may also have led to some small inconsistencies in material properties – potentially leading to further errors (not indicated by the included error bars which are derived from the recorded stress traces only). In addition, it is interesting to note that over the range of strain-rates / particle-velocities considered here, the high strain-rate response of Perma-Gel and muscle tissue both appear to be heading towards convergence.





However, the underlying deviation from the hydrodynamic curve for both sets of data suggests that caution would need to be employed in the un-restricted application of Perma-Gel® in its role as a muscle tissue analogue at higher strain-rates.

#### *4.2. Ballistic testing*

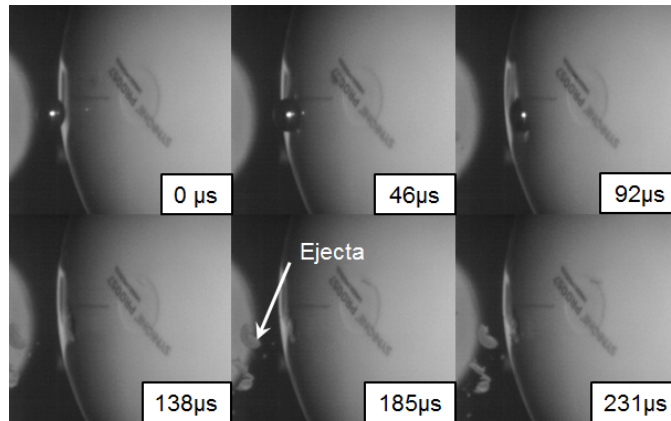
A series of four simplified ballistics tests were carried out in order to elucidate the dynamic material properties investigated in the aforementioned plate-impact experiments, as well as to expand on the limited previous ballistic investigations of Perma-Gel® conducted to-date [15, 16]. Due to the apparent convergence in behaviour between muscle tissue and Perma-Gel® in the  $\sigma_x$ - $u_p$  plane (Fig. 5), in contrast to the lack of such a correlation between muscle tissue and the more commonly employed simulant material Sylgard®, it was decided to investigate the ballistic response of both Sylgard® and Perma-Gel® in order to provide additional comparative data.

The experimental configurations which were based on the general setup illustrated previously in Fig. 2 are outlined in Table 4. In addition, post-impact photographs of (reassembled if required) targets are also included for each of the four tests in order to provide a ready comparison of the effects of differing target constructs.

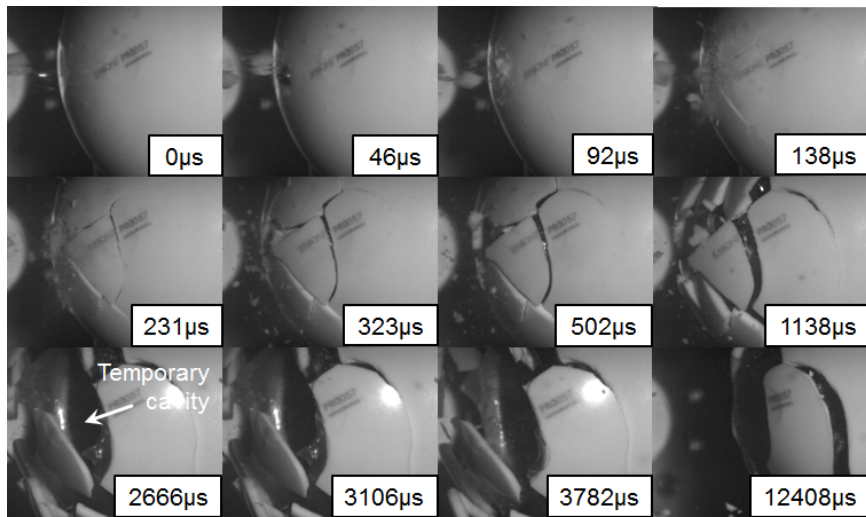
**Table 4.** Ballistic test configurations plus photographs of (reconstructed post-impact) Synbone® (porous polyurethane bone simulant) targets.

Impact velocity (m/s)	Target filling material	Post-impact images of (reconstructed) target Ø190 mm hemispheres
138	Perma-Gel®	
400	Perma-Gel®	
400	Empty	
400	Sylgard®	

A number of observations can immediately be made based on the four target configurations considered in Table 4. Firstly, the effects of strain-rate on the behaviour of a Perma-Gel® filled target become immediately apparent if the 138 and 400 m/s filled shots (corresponding to 68 and 572 J of impact energy respectively) are compared. At 138 m/s the projectile appears to have passed relatively cleanly through the target; however at 400 m/s significant Synbone® target disruption comprising a combination of radial and concentric cracks which led to target fragmentation out to approximately 2/3 of the target radius can be observed. From analysis of high-speed video footage for these 138 and 400 m/s Perma-Gel® shots, presented in Fig. 7, the difference in target behaviour for these two shots appeared to be linked to the elastomeric response of the underlying Perma-Gel®. At 138 m/s the strength of the Synbone® appeared to be sufficient to prevent any notable flexure due to oscillation of the backing Perma-Gel® fill, with only minor ejecta apparent – e.g. at 185 µs in Fig.7(a). Whereas at an impact velocity of 400 m/s oscillation of the Perm-Gel® post-impact was significantly more marked, leading to fracture of the Synbone® target surface. In this latter case, as shown in Fig. 7(b), radial cracks form initially (apparent from 92 µs), before concentric cracking occurs due to flexure / oscillation of the underlying Perma-Gel® (231 µs). This influence of the underlying backing material in causing eventual Synbone® failure is apparent by 2,666 µs, where a temporary cavity can be clearly observed which has led to delamination of the previously formed local Synbone® fragments.



(a)



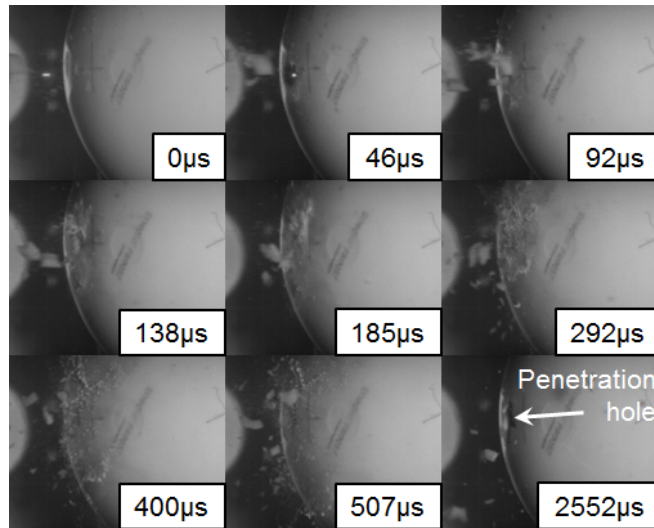
(b)

**Fig. 7.** Selected high-speed video frames illustrating 12-mm diameter stainless steel projectiles impacting a Perma-Gel® filled Synbone® hemisphere at differing impact velocities.

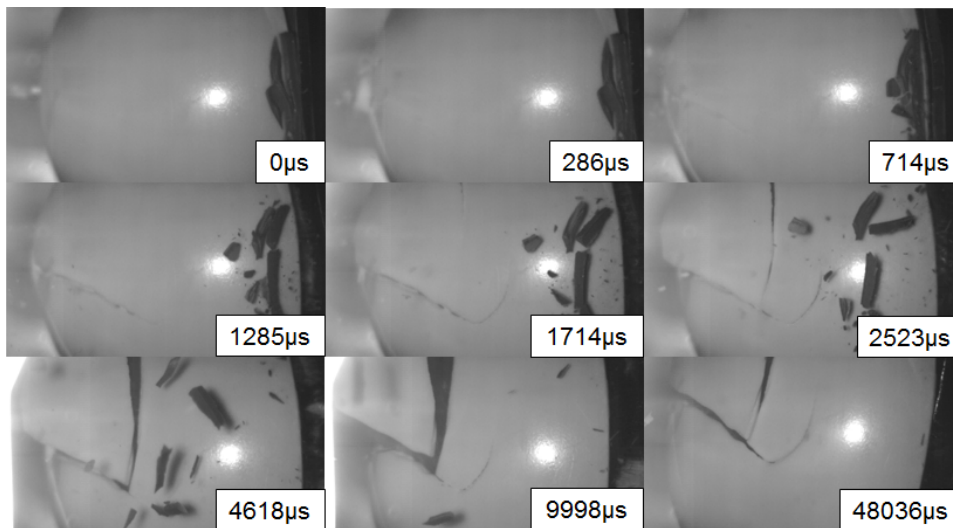
In addition to the effects of strain-rate, comparing the recovered target material for the 400 m/s Perma-Gel®, Synbone® and empty target cases in Table 4 the influence of the backing material properties on subsequent Synbone® failure can be clearly seen. For the empty target, penetration is interestingly less clean than for the supported 138 m/s event. However, the penetration hole is still only of the order of two projectile diameters in size and has not



led to extended Synbone® damage. However, the presence of either Perma-Gel® or Sylgard® (analogous to a ‘brain’ sitting within the Synbone® ‘skull’) leads to much more widespread post-impact Synbone® failure, with extensive radial and concentric cracking and subsequent target material (Synbone®) delamination. This effect is highlighted further in the high-speed video captured for the empty and Sylgard®-filled targets – presented in Figs. 8(a) and (b) respectively. In particular, while at extended times of several thousand microseconds in the empty target case in Fig. 8(a) no damage beyond that caused during the initial impact had occurred, for the supported target in Fig. 8(b) by 1,285  $\mu\text{s}$  radial cracking in the impacted Synbone® case is apparent. Further, it is interesting to note that such cracking occurs much sooner in the Perma-Gel® filled case under otherwise identical impact conditions; e.g. with radial cracks apparent by just 138  $\mu\text{s}$  in Fig. 7(b), c.a. ten times sooner after initial impact than in the Sylgard®-filled case shown in Fig. 8(b). This difference in material response is likely linked to the previously noted difference in dynamic properties of Perma-Gel® and Sylgard®; e.g. as identified from the  $U_s$ - $u_p$  Hugoniot data presented previously in Fig. 4, Sylgard® appears to be more compressible under high rates of loading than Perma-Gel®. It is postulated that this ability of Sylgard® to deform to a greater extent likely provides a route to dissipate incident energy, leading to observed the later onset of cracking of the Sylgard® (as opposed to Perma-Gel®) filled target. However, in both cases it is worth noting that final target disruption was overall comparable (e.g. Table 4) – suggesting that the Synbone® / Sylgard® or Perma-Gel® targets were overmatched by the impacting projectile in both 400 m/s cases.



(a)



(b)

**Fig. 8.** Selected high-speed video frames illustrating 12-mm diameter stainless steel projectiles impacting Synbone® hemispheres with differing fillings at 400 m/s.

Finally, it is worth noting that in addition to the insight provided into the filling materials themselves, this behaviour, with the response of Synbone® varying according to the backing medium employed, clearly illustrating the importance of employing multiple layers of appropriate analogue materials if accurate ballistic behaviour is to be simulated.

## 5. Conclusions

In this paper the high strain-rate and ballistic responses of the important epithelial / muscular tissue simulant Perma-Gel® have been characterised.

A series of seven plate-impact experiments allowed derivation of the Hugoniot equation-of-state for this material, with this information subsequently compared with literature data for both a comparable (brain) simulant Sylgard® and porcine muscle tissue. In the  $U_s$ - $u_p$  plane, the Hugoniot curve for Perma-Gel® exhibited marked curvature – something observed for other such polymeric materials and which was attributed to the multi-stage collapse of the inter-chain and inter-molecular bonds. Interestingly, Perma-Gel® was shown to exhibit a broadly similar compressibility to porcine muscle tissue under shock loading – with Sylgard® found to be significantly more pliant (compressible). In the  $\sigma_x$ - $u_p$  plane, a small degree of divergence of experimental data from the Hydrodynamic curve was apparent at elevated particle velocities. However, this apparent response was relatively slight, with the experimental data re-converging with the Hugoniot at elevated stresses (particularly when the data was observed in the  $\sigma_x$ - $v$  plane), suggesting that Perma-Gel® was essentially behaving hydrodynamically. The  $\sigma_x$ - $u_p$  Perma-Gel® data was also found to trend towards that of porcine muscle tissue at particle velocities of around 1 mm/ $\mu$ s, suggesting that Perma-Gel® was behaving differently to porcine material at lower impact velocities / stresses.

In addition to the plate-impact experiments, a series of four ballistic tests involving the impact of spherical projectiles on hemispherical Synbone® structures were carried out with the dual aims of (1) qualitatively confirming limited previous observations of the ballistic response of Perma-Gel® from the literature, and (2) identifying differences in ballistic response between Perma-Gel® and Sylgard®. Target configurations – comprising filled and

un-filled bone-simulant hemispheres were designed to nominally simulate a ‘head’ structure in line with one of the potential applications for such simulant materials (namely that of ‘brain’ tissue). These tests produced several key results. Firstly, in line with previous tests from the literature, Perma-Gel® was observed to behave elastomerically under impact. Secondly, analysis of both captured high-speed video footage and recovered Synbone® fragments clearly indicated that empty, Sylgard® filled and Perma-Gel® filled Synbone® targets all behaved differently under otherwise comparable impact conditions. Of particular note is the fact that inclusion of any filling medium – and the resultant constraint / effects on the encasing Synbone® during the penetration event – led to extensive radial and concentric cracking and subsequent target material delamination which was not apparent in the empty target case. Usefully, these ballistic tests also appeared to provide some evidence of a link between the hydrodynamic and ballistic response for both of the two key materials considered here – namely Perma-Gel® and Sylgard® – with this behaviour tentatively attributed to the materials differing high-rate compressibilities (evidenced by the measured  $U_s$ - $u_p$  Hugoniot data).

Overall, this study – via comparison of both the differing hydrodynamic response of Perma-Gel® to other tissue simulants and a limited series of ballistics tests – has demonstrated the importance of fully characterising the high strain-rate response of both tissue and analogue materials. In particular, it is apparent from comparison of the  $\sigma_x$ - $u_p$  and  $\sigma_x$ - $v$  equations-of-state for Perma-Gel® and muscle tissue that behaviour under high rates-of-strain can vary substantially with impact velocity / stress. E.g. here, a marked difference in Perma-Gel® and porcine muscle tissue response was apparent at low particle velocities, with a potential convergence under higher impact stresses, highlighting the fact that tissues and simulants may have differing responses to stimuli under different loading regimes. To this end, the equation-of-state data plus qualitative information on the ballistic response of Perma-Gel®

presented within this study should provide a useful basis for both practical and numerical (simulation) validation of its applicability as a potential tissue analogue.

## **Acknowledgements**

The primary author wishes to acknowledge the support of his wife, Caroline Appleby-Thomas, while writing this paper as well as the support from his daughters Mary-Ann and Phoebe and son, Michael. In addition, it is noted that the majority of the experimental work reported here was undertaken in the course of a Forensic Ballistics MSc undertaken by one of the authors, Miss Victoria Le-Seelleur, at Cranfield University's Shrivenham Campus in 2013/2014.

## **References**

- <sup>1</sup> Appleby-Thomas GJ, Hazell PJ, Stennett C, Cooper G, Helaar K, Diederer AM. Shock propagation in a cemented tungsten carbide. *J. Appl. Phys.* 2009;105(6):064916.
- <sup>2</sup> Nanda H, Appleby-Thomas GJ, Wood DC, Hazell PJ. Ballistic behaviour of explosively shattered alumina and silicon carbide targets. *Adv. in Appl. Ceram.* 2011;110(5):287-292.
- <sup>3</sup> Boteler JM, Dandekar DP. Dynamic response of two strain-hardened aluminum alloys. *J. Appl. Phys.* 2006;100:054902.
- <sup>4</sup> Nicholas NC, Welsch JR, Institute for Non-Lethal Defense Technologies Report: Ballistic Gelatin, Applied Research Laboratory, The Pennsylvania State University, USA (2004).
- <sup>5</sup> Shepherd CJ, Appleby-Thomas GJ, Hazell PJ, Allsop DF. The dynamic behaviour of ballistic gelatin. *AIP* 1195, Melville, New York, 1399-1402 (2009).
- <sup>6</sup> Appleby-Thomas GJ, Hazell PJ, Wilgeroth JM, Shepherd CJ, Wood DC, Roberts A. On the dynamic behavior of three readily available soft tissue simulants. *J. Appl. Phys.* 2011;109(8):084701-6.
- <sup>7</sup> Shepherd CJ, Appleby-Thomas GJ, Wilgeroth JM, Hazell PJ, Allsop DF. On the response of ballistic soap to one-dimensional shock loading. *Int. J. Impact Engng.* 2011;38(12):981-988.

- <sup>8</sup> Dyckmans G, Ndompetelo N, Chabotier A. Numerical and experimental study of the impact of small calibre projectiles on ballistic soap. *J. Phys. IV France* 2003;110:627-632.
- <sup>9</sup> Nsiampa N, Dyckmans, G, Chabotier, A. 2008. Numerical simulation of the tumbling effect of small caliber projectiles into ballistic soap. *Proceedings of the 8th World Congress on Computational Mechanics, Venice*.
- <sup>10</sup> Comley K, Fleck NA. The Toughness of Adipose Tissue: Measurements and Physical Basis. *J. Biomech.* 2010;43:1823-1826.
- <sup>11</sup> Jussila J, Leppäniemi A, Paronen M, Kulomäki E. Ballistic skin simulant. *Forensic Sci. Int.* 2005;150:63-71.
- <sup>12</sup> McElhaney JH. Dynamic response of bone and muscle tissue. *J. Appl. Physiol.* 1966;21:1231-1236.
- <sup>13</sup> Ural A, Zioupos P, Buchanan D, Vashishth D. The effect of strain rate on fracture toughness of human cortical bone: A finite element study. *J. Mech. Behavior of Biomed. Mater.* 2011;4:1021-1032.
- <sup>14</sup> Roberts MVB, *Biology. A Functional Approach*, Cox and Wyman Ltd., London, UK (1973).
- <sup>15</sup> Ryckman RA, Powell DA, Lew AJ. Ballistic Penetration of Perma-Gel. *AIP Conf. Proc.* 1426, 143-148 (2012).
- <sup>16</sup> Mabbott A, Carr DJ, Champion S, Malbon C, Tichler C. Comparison of 10% Gelatine, 20% Gelatine and Perma-Gel™ for Ballistic Testing. *Proc. of the 27<sup>th</sup> Int. Symp. on Ballistics, Freidburg (Germany), 22-26 April, 648-654* (2013).
- <sup>17</sup> Pervin F, Chen WW. Mechanically Similar Gel Simulants for Brain Tissues. *Proc. of the SEM Annual Conf., Indianapolis (US), 7-10 June, 9* (2010).
- <sup>18</sup> Appleby-Thomas GJ, Hazell PJ, Cleave R. Penetration mechanisms in glass laminate/resin structures. *Mater. and Design* 2012;34:541-551.
- <sup>19</sup> Kalcioğlu ZI, Qu M, Strawhecker KE, Shazly T, Edelman E, VanLandingham MR, Smith JF, Van Vliet KJ. Dynamic impact indentation of hydrated biological tissues and tissue surrogate gels. *Phil. Mag.* 2011;91(7-9):1339-1355.
- <sup>20</sup> Meyers MA. *Dynamic Behavior of Materials*, John Wiley & Sons, Inc., New York, USA (1994).
- <sup>21</sup> Field JE, Walley SM, Proud WG, Goldrein HT, Siviour CR. Review of experimental techniques for high rate deformation and shock studies. *Int. J. Impact Engng.* 2004;30:725-775.
- <sup>22</sup> Hazell PJ, Appleby-Thomas GJ, Wielewski E, Stennett C, Siviour C. The influence of microstructure on the shock and spall behaviour of the magnesium alloy, Elektron 675. *Acta Materialia* 2012;60(17):6042-6050.
- <sup>23</sup> Appleby-Thomas GJ, Hazell PJ, Sheldon RP, Stennett C, Hameed A, Wilgeroth JM. The high strain-rate behaviour of selected tissue analogues. *J. Mech. Behavior of Biomed. Mater.* 2014;33:124-135.

- <sup>24</sup> Wilgeroth JM, Hazell PJ, Appleby-Thomas GJ. On the behaviour of porcine skeletal muscle tissue under shock compression. *Int. J. Impact Engng.* 2012;50:83-89.
- <sup>25</sup> Rosenberg Z, Yaziv D, and Partom Y. Calibration of foil-like manganin gauges in planar shock wave experiments. *J. Appl. Phys.* 1980;51(7):3702-3705.
- <sup>26</sup> Hazell PJ, Stennett C, and Cooper G. The shock and release behavior of an aerospace-grade cured aromatic amine epoxy resin. *Polymer Comp.* 2008;29(10):1106-1110.
- <sup>27</sup> Munson DE, May RP. Dynamically determined high-pressure compressibilities of three epoxy resin systems. *J. Appl. Phys.* 1972;43(3):962-971.
- <sup>28</sup> Barker LM, Hollenbach RE. Shock-wave studies of PMMA, fused silica and sapphire. *J. Appl. Phys.* 1970;41(10):4208-4226.
- <sup>29</sup> Porter D, Gould PJ. A general equation of state for polymeric materials. *J. Physique IV* 2006;134:373-378.
- <sup>30</sup> Davison L, Graham RA. Shock Compression of Solids. *Physics Reports (Review Section of Physics Letters)* 1979;55(4):255-379.
- <sup>31</sup> Millett JCF, Bourne NK, Meziere YJE, Vignjevic R, Lukyanov A. The effect of orientation on the shock response of a carbon fibre-epoxy composite. *Compos. Sci. and Tech.* 2007;67:3253-3260.
- <sup>32</sup> Bourne NK, Millett JCF. On the influence of chain morphology on the shock response of three thermoplastics. *Metallurgical and Mater. Trans. A: Physical Metallurgy and Mater. Sci.* 2008;39(2):266-271.
- <sup>33</sup> Millett JCF, Bourne NK, Gray III GT. The response of polyether ether ketone to one-dimensional shock loading. *J. Phys. D: Appl. Phys.* 2004;37(6):942-947.
- <sup>34</sup> Bourne NK, Millett JCF. Tacticity in shocked polymer hydrocarbons. *J. Mater. Sci.* 2008;43(1):185-189.
- <sup>35</sup> Appleby-Thomas GJ, Hazell PJ, Stennett C. The variation in lateral and longitudinal stress gauge response within an RTM 6 epoxy resin under one-dimensional shock loading. *J. Mater. Sci.* 2009;44:6187-6198.
- <sup>36</sup> Housecroft CE, Constable EC. *Chemistry: An Introduction to Organic, Inorganic and Physical Chemistry*, 3<sup>rd</sup> ed., Pearson Education Ltd., Harlow, UK (2006).
- <sup>37</sup> Davison L. *Fundamentals of Shock Wave Propagation in Solids*, Springer-Verlag, Berlin, Germany (2008).